Compressive Sampling for Detection of Frequency-Hopping Spread Spectrum Signals

Feng Liu, Michael W. Marcellin, *Fellow, IEEE*, Nathan A. Goodman, *Senior Member, IEEE*, and Ali Bilgin, *Senior Member, IEEE*

***Abstract*—In this paper, methods for detection of frequency-hopping spread spectrum (FHSS) signals from compressive measurements are proposed. Rapid switching of the carrier frequency in a pseudorandom manner makes detection of FHSS signals challenging. Conventionally, FHSS detection is performed by scanning small segments of the spectrum in a sequential manner using a sweeping spectrum analyzer (SSA). However, SSAs have the inherent risk of missing the transmitted signal depending on factors such as the rate of hopping and scanning. In this paper, we propose compressive detection strategies that sample the full FHSS spectrum in a compressive manner. We discuss the use of random measurement kernels as well as designed measurement kernels in the proposed architecture. The measurement kernels are designed to maximize the mutual information between the FHSS signal and the compressive measurements. Using a mixture-of-Gaussian model to represent the FHSS signal, we derive a closed-form gradient of the mutual information with respect to the measurement kernel. Theoretical analysis and simulation results are provided to compare different systems. These results demonstrate that the proposed compressive system with random measurement kernels is not subject to the performance limitations suffered by SSAs when their scanning rates are low and designed adaptive measurement kernels provide enhanced detection performance compared to random ones.**

***Index Terms*—Spread spectrum, FHSS, sweeping spectrum analyzer (SSA), compressive detection, mutual information, adaptive detection.**

I. Introduction

FREQUENCY-hopping spread spectrum (FHSS) is a spread spectrum (SS) modulation technique used in communication systems [1]. In FHSS, the spectrum of the signal is spread by switching the carrier frequency in a pseudo-random manner. The pseudo-random switching sequence used by the transmitter is known to a cooperative receiver and, thus, the transmitter/receiver pair can communicate in synchronization using the same carrier frequency. The rapidly switching carrier frequency of FHSS systems enables several desirable attributes: first, the instantaneous interference from FHSS signals to other signals is often insignificant since the period of interference is limited by the hopping period. Similarly, the FHSS signals are also resistant to interference from other signals since they do not occupy a fixed frequency range for extended periods. This property also makes FHSS signals resistant to jamming. Finally, the rapid switching of the carrier frequency makes detection of FHSS signals challenging as well. Since the FHSS signals can hop over very large bandwidths, the observation of such large bandwidths for signal detection presents significant challenges to conventional detectors.

Although many novel detection methods (e.g. autocorrelation based [2]–[5], wavelet-based [2], [6]–[10], likelihood based [11]–[16], time-frequency feature analysis based [6], [17]–[21]) have been proposed in the literature, the most common method for detection of FHSS signals is to use channelized radiometers to measure signal energy [22]–[24]. A typical radiometer uses a bandpass filter to select the frequency band over which measurements are made. Since FHSS signals hop over large frequency ranges, energy measurements are needed over these large bandwidths. If the FHSS signal can be sampled at a high enough rate to capture the full FHSS bandwidth, a digital filterbank can be used to detect energy in each channel. However, capturing the entire FHSS bandwidth often requires very high-rate analog-to-digital converters. A common method to measure energy over a large frequency range is to use a sweeping spectrum analyzer (SSA) [15], [25]–[29]. An SSA sequentially scans frequency bands and measures signal energy in each frequency band. However, the detection performance of the SSA is highly dependent on its scanning rate and the hopping rate of the FHSS signal. If the scanning rate of the SSA is not high enough, the scanning support can miss the hopping signal.

In this paper, motivated by the recent *compressive sensing* (CS) theory [30], [31], we propose methods for detection of FHSS signals from compressive measurements. While most of the compressive sensing methods aim to reconstruct a signal by exploiting its sparsity, our goal is to detect the presence of the FHSS signals. Several methods for compressive detection were proposed in the literature over the last decade [32]–[38]. Some of these methods assume that the signal can be sparsely represented in known dictionaries [33], [35], [37], [38]. Others assume precise knowledge of the signal [32] or propose to learn the signal sparsity model from training signals [34]. The compressive detection methods in this paper are based on energy detection and only require knowledge of the signal variance.

Manuscript received January 14, 2015; revised October 12, 2015 and July 1, 2016; accepted July 20, 2016. Date of publication August 2, 2016; date of current version September 8, 2016. The associate editor coordinating the review of this manuscript and approving it for publication was Prof. Sergios Theodoridis. This work was supported by the Defense Advanced Research Projects Agency Knowledge Enhanced Compressive Measurements Project under contract #N66001-10-1-4079. Part of this work was presented at the 2013 SPIE Defense, Security, and Sensing Conference [54].

F. Liu and M. W. Marcellin are with the Department of Electrical and Computer Engineering, University of Arizona, Tucson, AZ 85721 USA (e-mail: liuf@email.arizona.edu; mwm@email.arizona.edu).

N. A. Goodman is with the School of Electrical & Computer Engineering, University of Oklahoma, Norman, OK 73019 USA (e-mail: goodman@ou.edu).

A. Bilgin is with the Department of Biomedical Engineering and the Department of Electrical and Computer Engineering, University of Arizona, Tucson, AZ 85721 USA (e-mail: bilgin@email.arizona.edu).

Digital Object Identifier 10.1109/TSP.2016.2597122

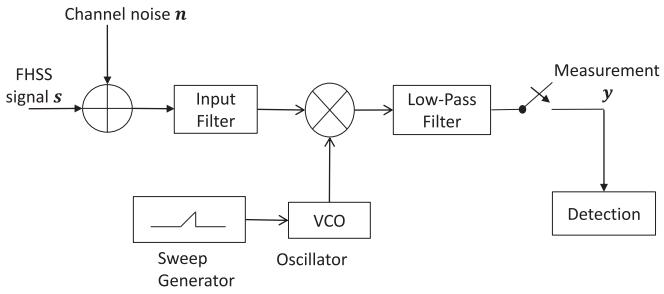

Fig. 1. Block diagram of a scanning spectrum analyzer.

Similar to [32], our methods work directly on the compressive measurements and do not require an intermediate step of signal recovery. While most of the compressive detection methods in the literature use dense matrices for sampling, the use of sparse random projections for compressive detection was also proposed recently [38]. In this work, we used block-diagonal sensing matrices similar to those proposed in [39] for signal recovery problems. The resulting compressive detection architecture has comparable hardware cost to the SSA-based systems. It utilizes wideband measurement kernels but performs compressive measurements such that the data acquisition rate of the proposed system is similar to that of SSA-based systems. However, the proposed system is not subject to the performance limitations suffered by SSAs when their scanning rates are low. We discuss the use of random measurement kernels as well as designed measurement kernels in the proposed architecture. It should be noted that compressive detection methods for multiple access have also been introduced recently [40]–[43]. While the analysis in this work focuses on the single-user detection setting and the use of designed measurement kernels, extension of this framework to multi-user setting is also possible [44].

The remainder of this paper is organized as follows: in Section II, the conventional SSA systems are discussed and a model to analyze the theoretical performance of these systems is developed. In Section III, our proposed compressive detection method is introduced. A method for designed compressive measurement kernel design is proposed in Section IV. Theoretical and experimental results are presented in Section V. Finally, Section VI provides a summary and the conclusions.

II. Detection of FHSS Signals using SSAs

As discussed in the previous section, energy detection using SSAs is arguably the most common method for detection of FHSS signals [29]. In this section, we develop a model to analyze the theoretical detection performance of SSA-based energy detection. The block diagram of a typical SSA is shown in Fig. 1. Here, the input signal is mixed with the signal from a voltage controlled oscillator (VCO). The mixed signal is passed through a low-pass filter and the filter output is sampled with the Nyquist rate with respect to the passband of the low-pass filter. The samples are used to detect the presence or absence of FHSS signals. By sweeping the frequency of the VCO signal, SSA scans different frequency subbands.

An FHSS signal can be represented as:

$$s(t) = A(t)e^{j(2\pi f_{\rm c}(t))} \tag{1}$$

where $A(t)$ denotes the signal in baseband and $f_{\rm c}(t)$ denotes the time-varying carrier frequency. By changing the carrier frequency $f_{\rm c}(t)$ randomly at certain time intervals, the FHSS signal switches among many frequency channels. Let B denote the full frequency hopping range of the FHSS signal. Let's also assume that the SSA uniformly divides this range into $N_{\rm b}$ subbands which are scanned sequentially. Then, the Nyquist sampling rate used to scan each subband is computed with respect to the bandwidth of each subband $B/N_{\rm b}$. Let α denote the relative scanning rate which is defined as the number of scanning intervals per FHSS hopping period. Mathematically, α can be expressed as:

$$\alpha = \frac{N_{\rm s}}{N_{\rm h}} \tag{2}$$

where $N_{\rm s}$ denotes the number of subbands scanned within a given time period and $N_{\rm h}$ denotes the number of frequency hops during the same period. Note that when $\alpha \geq N_{\rm b}$, SSA scans the entire hopping frequency range before the FHSS signal hops. We refer to this regime as the *fast scanning regime*. Conversely, when $\alpha < N_{\rm b}$, the signal hops before the SSA scans the entire hopping frequency range. We refer to this regime as the *fast hopping regime*. To simplify our analysis, we assume that α is either a rational number of 1 divided by a positive integer or a positive integer that can divide or be divided by $N_{\rm b}$.

During the ith scanning interval, the relationship between the measurement vector $\mathbf{y}_i$ and the FHSS signal $\mathbf{s}_i$ can be modeled by:

$$\mathbf{y}_i = \mathbf{\Phi}_i(\mathbf{s}_i + \mathbf{n}_i) \tag{3}$$

where $\mathbf{n}_i$ denotes the additive channel noise and $\mathbf{\Phi}_i$ denotes the matrix representation of the measurement kernel during the $i^{\rm th}$ scanning interval. Here, measurements are obtained by applying a bandpass filter to the noisy input signal so the matrix $\mathbf{\Phi}_i$ represents this bandpass filtering process. In this discretized notation, if the signal $\mathbf{s}_i$ is discretized at the Nyquist rate corresponding to the full hopping bandwidth to yield N samples and M measurements are made during the $i^{\rm th}$ scanning interval, the matrix $\mathbf{\Phi}_i$ will have the dimensions $M \times N$. The channel noise $\mathbf{n}_i$ is modeled as complex zero-mean additive white Gaussian noise with variance $\sigma_{\rm n}^2$ covering the entire FHSS hopping range. To simply our derivations, $\mathbf{s}_i$ is modeled as a complex zero-mean Gaussian white signal with variance $\sigma_{\rm s}^2$ within the scanning support that it falls in.

During each scanning period, the decision on the presence or absence of the FHSS signal can be made based on energy detection. This detection problem can be formulated as a choice between two hypotheses:

$$H_{0,i} : \mathbf{y}_i = \mathbf{\Phi}_i \mathbf{n}_i \tag{4}$$

$$H_{1,i} : \mathbf{y}_i = \mathbf{\Phi}_i(\mathbf{s}_i + \mathbf{n}_i) \tag{5}$$

where $H_{0,i}$ and $H_{1,i}$ denote the signal absent and signal present hypotheses in the $i^{\rm th}$ scanning interval, respectively. Given the

detection decisions made in all scanning intervals, the final detection decision is made after the entire FHSS hopping range is observed. If the decision "signal present" is made in at least one of the scanning intervals, the final decision "signal present" is made; otherwise, the final decision "signal absent" is made.

Let $\lambda_i = \|\mathbf{y}_i\|_2^2$ denote the measurement energy during the ith scanning interval where $\|\cdot\|_2^2$ denotes the squared 2-norm operation. Assuming that the low-pass filter in Fig. 1 is ideal, the variance of the input signal is preserved in the measurement since $\mathbf{\Phi}_i$ is row-wise orthonormal, i.e., $\mathbf{\Phi}_i^\dagger \mathbf{\Phi}_i = \mathbf{I}_M$, where $\cdot^\dagger$ represents the conjugate transpose (Hermitian) operation and $\mathbf{I}_M$ denotes the $M \times M$ identity matrix. Then λ_i is the sum of the energies of M independent and identically distributed (i.i.d.) zero-mean circularly-symmetric Gaussian complex random variables with the variances of σ_{n}^2. Equivalently, λ_i cab also be expressed as the sum of squares of $2M$ i.i.d. zero-mean Gaussian real random variables with variances $\frac{\sigma_{\mathrm{n}}^2}{2}$. Let $E_i = \frac{2\lambda_i}{\sigma_{\mathrm{n}}^2}$. E_i is central χ-squared distributed with $2M$ degrees of freedom [45]:

$$p(E_i|H_{0,i}) = \frac{{E_i}^{(M-1)} e^{-\frac{E_i}{2}}}{2^M \Gamma(M)} \tag{6}$$

where $\Gamma(\cdot)$ denotes the gamma function. Thus, the distribution of λ_i when the signal is absent is given by:

$$p(\lambda_i|H_{0,i}) = \frac{(\frac{2\lambda_i}{\sigma_{\mathrm{n}}^2})^{(M-1)} e^{-\frac{\frac{2\lambda_i}{\sigma_{\mathrm{n}}^2}}{2}}}{2^M \Gamma(M)} \cdot \frac{2}{\sigma_{\mathrm{n}}^2} = \frac{{\lambda_i}^{(M-1)} e^{-\frac{\lambda_i}{{\sigma_{\mathrm{n}}}^2}}}{{\sigma_{\mathrm{n}}}^{2M} \Gamma(M)}. \tag{7}$$

Using the distribution in (7), the theoretical false positive rate (FPR) during the i^{th} scanning interval is calculated by:

$$\mathrm{FPR}_i = \int_{T_i}^{+\infty} p(\lambda_i|H_{0,i}) d\lambda_i \tag{8}$$

where T_i denotes the detection threshold used during the i^{th} scanning interval. The overall theoretical FPR (i.e. the FPR associated with the final detection decision after all N_{b} subbands are scanned) is then calculated by:

$$\mathrm{FPR} = 1 - \mathrm{TNR} = 1 - \prod_{i=1}^{N_{\mathrm{b}}} \mathrm{TNR}_i = 1 - \prod_{i=1}^{N_{\mathrm{b}}} (1 - \mathrm{FPR}_i) \tag{9}$$

where TNR_i denotes the theoretical true negative rate (TNR) during the i^{th} scanning interval.

When the signal is present, the overall false negative rate (FNR) depends on the relative scanning rate α. If the scanning rate is not faster than the FHSS hopping rate (i.e., $\alpha \leq 1$), the scanning intervals are independent. The distribution of the measurement energy during the i^{th} scanning interval is then calculated as:

$$p(\lambda_i|H_{1,i}) = \sum_{k=0}^{\frac{1}{\alpha}} \binom{\frac{1}{\alpha}}{k} (p_i)^k (1-p_i)^{\frac{1}{\alpha}-k} \frac{{\lambda_i}^{(M-1)} e^{-\frac{\lambda_i}{\alpha k N_{\mathrm{b}} {\sigma_{\mathrm{s}}}^2 + {\sigma_{\mathrm{n}}}^2}}}{(\alpha k N_{\mathrm{b}} {\sigma_{\mathrm{s}}}^2 + {\sigma_{\mathrm{n}}}^2)^M \Gamma(M)} \tag{10}$$

where p_i denotes the probability that the i^{th} subband is occupied by the FHSS signal at any given time. Mathematically,

$$p_i = Pr\left(f_{\min} + \frac{(i-1)\cdot B}{N_{\mathrm{b}}} < f_{\mathrm{c}}(t) < f_{\min} + \frac{i \cdot B}{N_{\mathrm{b}}} \right) \tag{11}$$

where $f_{\min}$ denotes the lower bound of the frequency hopping range.

Note that when $\alpha \leq 1$, the FHSS signal can occupy the scanned subband multiple times during a scanning interval and, therefore, $p(\lambda_i|H_{1,i})$ becomes a mixture of chi-squared distributions as shown in (10). Using the distribution in (10), the theoretical FNR during the i^{th} scanning interval is given by:

$$\mathrm{FNR}_i = \int_{-\infty}^{T_i} p(\lambda_i|H_{1,i}) d\lambda_i. \tag{12}$$

The overall theoretical FNR (i.e. the FNR associated with the final detection decision after all N_{b} subbands are scanned) is then given by:

$$\mathrm{FNR} = \prod_{i=1}^{N_{\mathrm{b}}} \mathrm{FNR}_i. \tag{13}$$

Next, we consider the case when $1 < \alpha < N_{\mathrm{b}}$. In this case, the scanning rate is fast enough to cover multiple subbands during a single hopping period. More specifically, the SSA can scan α subbands before the FHSS signal hops. We can therefore consider that the entire set of N_{b} subbands are divided into $\frac{N_{\mathrm{b}}}{\alpha}$ groups with α subbands each. We refer to these as *scan groups*. Let j denote the scan group index. Since there are $\frac{N_{\mathrm{b}}}{\alpha}$ scan groups, $j \in \{1, 2, \ldots, \frac{N_{\mathrm{b}}}{\alpha}\}$. Similarly, we will use i to denote the subband (or equivalently scanning interval) index. Since there are N_{b} subbands, $i \in \{1, 2, \ldots, N_{\mathrm{b}}\}$. It can be seen that subbands $i = 1, 2, \ldots, \alpha$ will be scanned during scan group $j = 1$, subbands $i = \alpha + 1, \alpha + 2, \ldots, 2\alpha$ will be scanned during scan group $j = 2$, and so on. Let us denote the FNR during j^{th} scan group as $\mathrm{FNR}_{\mathrm{g},j}$ where the subscript "g" denotes "group". In order to calculate this value, we need to consider two cases: When the signal falls within the support of the j^{th} scan group and when it falls out of this support during the time period associated with the j^{th} scan group. In our subsequent notation, we will use "gp" to denote "group when signal present" and "ga" to denote "group when signal absent." Let us denote the FNR corresponding to each of these cases using $\mathrm{FNR}_{\mathrm{gp},j}$ and $\mathrm{FNR}_{\mathrm{ga},j}$, respectively. Then the FNR during the j^{th} scan group can be expressed as:

$$\mathrm{FNR}_{\mathrm{g},j} = \mathrm{FNR}_{\mathrm{gp},j} + \left[1 - \sum_{i=(j-1)\alpha+1}^{j\alpha} p_i \right] \mathrm{FNR}_{\mathrm{ga},j}. \tag{14}$$

In (14), the term $[1 - \sum_{i=(j-1)\alpha+1}^{j\alpha} p_i]$ corresponds to the probability of the signal being outside the support of the j^{th} scan group. When the signal is within the support of the j^{th} scan group, it will occupy one of the subbands $((j-1)\alpha + 1)^{\text{th}}$

through $j\alpha^{\text{th}}$. Therefore, we can express $\text{FNR}_{\text{gp},j}$ as:

$$\text{FNR}_{\text{gp},j} = \sum_{i=(j-1)\alpha+1}^{j\alpha} p_i \text{FNR}_{\text{gp},i,j} \tag{15}$$

where $\text{FNR}_{\text{gp},i,j}$ denotes the FNR when the signal falls into the support of the i^{th} scanning interval during the time interval of the j^{th} scan group. $\text{FNR}_{\text{gp},i,j}$ can be calculated as the product of two terms:

$$\text{FNR}_{\text{gp},i,j} = \text{FNR}'_{\text{gp},i,j} \cdot \text{FNR}''_{\text{gp},i,j}. \tag{16}$$

Here, $\text{FNR}'_{\text{gp},i,j}$ denotes the FNR when the signal falls within the i^{th} subband during the j^{th} scan group and $\text{FNR}''_{\text{gp},i,j}$ denotes the FNR when the signal falls within one of the other subbands (i.e. subbands $k \in \{(j-1)\alpha+1, \ldots, j\alpha\}, k \neq i$) within the support of the j^{th} scan group. These quantities can be calculated as:

$$\text{FNR}'_{\text{gp},i,j} = \int_{-\infty}^{T_i} \frac{{\lambda_i}^{(M-1)} e^{-\frac{\lambda_i}{N_{\text{b}}{\sigma_{\text{s}}}^2 + {\sigma_{\text{n}}}^2}}}{(N_{\text{b}}{\sigma_{\text{s}}}^2 + {\sigma_{\text{n}}}^2)^M \Gamma(M)} d\lambda_i \tag{17}$$

and

$$\text{FNR}''_{\text{gp},i,j} = \prod_{k=(j-1)\alpha+1}^{j\alpha} \int_{-\infty}^{T_k} \frac{{\lambda_k}^{(M-1)} e^{-\frac{\lambda_k}{{\sigma_{\text{n}}}^2}}}{{\sigma_{\text{n}}}^{2M} \Gamma(M)} d\lambda_k \quad k \neq i \tag{18}$$

respectively. Similarly, $\text{FNR}_{\text{ga},j}$ can be calculated as:

$$\text{FNR}_{\text{ga},j} = \prod_{i=(j-1)\alpha+1}^{j\alpha} \int_{-\infty}^{T_i} \frac{{\lambda_i}^{(M-1)} e^{-\frac{\lambda_i}{{\sigma_{\text{n}}}^2}}}{{\sigma_{\text{n}}}^{2M} \Gamma(M)} d\lambda_i, \tag{19}$$

since it is the FNR corresponding to when the signal is not within the support of the j^{th} scan group. The overall theoretical FNR (after all scan groups have been scanned) for this case is given by:

$$\text{FNR} = \prod_{j=1}^{\frac{N_{\text{b}}}{\alpha}} \text{FNR}_{\text{g},j}. \tag{20}$$

Finally, we consider the case when the scanning rate is much faster than the hopping rate such that the scanner can scan all N_b subbands before the signal hops. In this case, $\alpha \geq N_{\text{b}}$. It is easy to see that this case can be considered as having a single scan group which contains all subbands. Therefore, the FNR in this case can be obtained by setting $j = 1$ and $\alpha = N_{\text{b}}$ in (15). This yields:

$$\text{FNR} = \sum_{i=1}^{N_{\text{b}}} p_i \text{FNR}_{\text{gp},i,1}. \tag{21}$$

The FPR and FNR calculated in this section can be used to evaluate the detection performance of SSAs. As we will illustrate in Section V, SSAs suffer from a "floor" problem in their FNR when $\alpha < N_{\text{b}}$. This floor is due to the non-zero probability that the SSA misses the hopping signal if the scanning rate of the SSA is not fast enough to cover the entire hopping range before the signal hops. A detailed evaluation of this floor problem is presented in Section V.

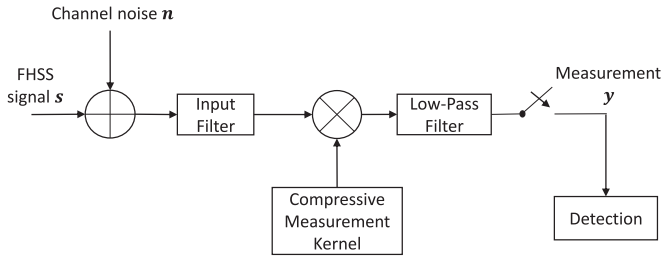

Fig. 2. Block diagram of the proposed compressive detector.

III. Compressive Detection of FHSS Signals

The recent CS theory, as presented in the seminal works of Candes *et al.* [30] and Donoho [31], provides a novel perspective on sufficient sampling. This new perspective resulted in extensive research on compressive systems over the past decade. Motivated by the CS theory, we investigate compressive approaches to detect the presence or absence of FHSS signals in this work. We start this section by introducing our compressive detection framework. The block diagram of the proposed framework is shown in Fig. 2. In this architecture, the noisy input signal is mixed with wide-band measurement kernels and passed through a low-pass filter. The output of the low-pass filter is sampled at a rate much lower than the one suggested by the Nyquist sampling theorem for the full FHSS hopping bandwidth. Therefore, this measurement system is compressive. The compressive measurements are then used to detect the presence or absence of FHSS signals. It is worth pointing out that this architecture is very similar to the SSA architecture shown in Fig. 1 with the exception that the measurements are obtained using wide-band measurement kernels in this case whereas the SSA uses band-limited measurement kernels. Similar compressive measurement structure was also used in [39] to sense the input signal compressively with different kinds of measurement kernels discussed. In contrast, the sparsity of the signal was observed and CS algorithms were discussed in [39] in order to reconstruct the signal from the compressive measurements.

In this framework, the relationship between the measurement vector $\mathbf{y}$ and the signal $\mathbf{s}$ can be modeled by

$$\mathbf{y} = \mathbf{\Phi}(\mathbf{s} + \mathbf{n}) \tag{22}$$

where $\mathbf{n}$ denotes the complex additive white Gaussian channel noise with zero-mean and variance σ_{n}^2 over the entire SS range.

In our analysis, we divide the measurement process into N_{b} sequential observation intervals. Note that the proposed compressive detection method can work with any number of measurements and this division of the measurement process into sequential observation intervals is not strictly necessary. However, we analyze the performance of the proposed method under these conditions to allow a fair comparison with the SSA-based system. During each observation interval i, the measurements, the signal, and the channel noise are denoted by $\mathbf{y}_i$, $\mathbf{s}_i$ and $\mathbf{n}_i$ respectively. Naturally, by concatenating $\mathbf{y}_i$ for $1 \leq i \leq N_{\text{b}}$, the full measurement vector $\mathbf{y}$ can be obtained. Similarly, the signal vector $\mathbf{s}$ and the noise vector $\mathbf{n}$ can be obtained by concatenating vectors $\mathbf{s}_i$ and $\mathbf{n}_i$, respectively, for $1 \leq i \leq N_{\text{b}}$. During each observation interval, the complex $M \times N$ measurement

kernel is denoted by $\mathbf{\Phi}_i$. The full measurement matrix $\mathbf{\Phi}$ is a $MN_\mathrm{b} \times NN_\mathrm{b}$ block-diagonal matrix where the diagonal blocks consist of $\mathbf{\Phi}_i$ for $1 \leq i \leq N_\mathrm{b}$.

The detection problem can be formulated as a decision between two hypothesis:

$$H_0 : \mathbf{y} = \mathbf{\Phi}\mathbf{n} \tag{23}$$

$$H_1 : \mathbf{y} = \mathbf{\Phi}(\mathbf{s} + \mathbf{n}) \tag{24}$$

where H_0 and H_1 denote the signal absent and signal present hypotheses, respectively.

Since we are interested in compressive measurements, it is worth defining the compression ratio (CR) in this setting. Given that N is the number of samples needed to sample the signal at the Nyquist rate and M is the number of measurements during each observation interval, the CR is given by $CR = \frac{N}{M}$. For the measurement system shown in Fig. 2, the measurement matrix in each observation interval, $\mathbf{\Phi}_i$, is block-diagonal where each block is a $1 \times CR$ vector.

Most of the existing CS signal recovery methods rely on random measurement kernels since random measurement kernels yield, with high probability, incoherent measurements with any sparsity domain. In our compressive detection framework, random measurements can be obtained by randomly selecting the non-zero entries of the measurement matrix $\mathbf{\Phi}$. Assuming such $\mathbf{\Phi}$ with normalized rows and modeling the FHSS signal $\mathbf{s}$ as a complex zero-mean Gaussian white signal with the variance σ_s^2, the measurements are i.i.d. Gaussian and, therefore, the distribution of measurement energy, which is defined as $\lambda = \|\mathbf{y}\|_2^2$, follows the central chi-squared distribution for the signal absent case:

$$p(\lambda|H_0) = \frac{\lambda^{(MN_\mathrm{b}-1)} e^{-\frac{\lambda}{{\sigma_\mathrm{n}}^2}}}{{\sigma_\mathrm{n}}^{2MN_\mathrm{b}}\Gamma(MN_\mathrm{b})}. \tag{25}$$

Similar to (25), the distribution of the measurement energy λ for the signal present case follows the central chi-squared distribution given by:

$$p(\lambda|H_1) = \frac{\lambda^{(MN_\mathrm{b}-1)} e^{-\frac{\lambda}{({\sigma_\mathrm{s}}^2+{\sigma_\mathrm{n}}^2)}}}{({\sigma_\mathrm{s}}^2+{\sigma_\mathrm{n}}^2)^{MN_\mathrm{b}}\Gamma(MN_\mathrm{b})}. \tag{26}$$

Given a threshold T, the theoretical FPR of this compressive detection system is calculated by:

$$\mathrm{FPR} = \int_T^+ p(\lambda|H_0)d\lambda \tag{27}$$

and the theoretical FNR is calculated by:

$$\mathrm{FNR} = \int_{-\infty}^T p(\lambda|H_1)d\lambda. \tag{28}$$

From (27) and (28), we can see that the performance of our proposed compressive detection system does not depend on the relative measurement rate α. This is an important advantage of the proposed compressive detection system over the SSA based detection systems. Results shown in Section V will quantify this advantage.

IV. Knowledge Enhanced Compressive Detection of FHSS Signals

In the previous section, a compressive detection framework using random measurement kernels was proposed. While most of the CS literature uses random measurement kernels, there is existing work [46], [47] which illustrates that compressive measurement kernels designed using prior knowledge of the signal and the measurement system can improve performance. Motivated by [46], [47], we extend our compressive detection framework to consider the use of designed measurement kernels in this section.

Specifically, we propose to design measurement kernels that maximize the mutual information between the FHSS signal and the measurements. This design procedure can be described as follows: recall from Section III that the measurement process is divided into N_b sequential observation intervals. During the observation interval i, the $M \times N$ measurement kernel is denoted by $\mathbf{\Phi}_i$. As illustrated in Section III, only a small fraction of the entries in each row of $\mathbf{\Phi}_i$ are non-zero. Let $\mathbf{\Phi}_{i,m}$ denote the non-zero entries in the m^{th} row of this measurement matrix $\mathbf{\Phi}_i$. Let $\mathbf{s}_{i,m}$, $\mathbf{n}_{i,m}$ and $y_{i,m}$ denote the signal, the noise, and the measurement, respectively, during the time interval corresponding to $\mathbf{\Phi}_{i,m}$. Similar to the random compressive measurement kernel, we add one additional constraint in the optimization process that $\mathbf{\Phi}_{i,m}$ is normalized. The goal of measurement kernel design is to obtain $\mathbf{\Phi}_{i,m}$ such that:

$$\begin{aligned}\mathbf{\Phi}_{i,m} &= \arg\max_{\hat{\mathbf{\Phi}}_{i,m}} I(y_{i,m};\mathbf{s}_{i,m}) \\ \text{s.t. } y_{i,m} &= \hat{\mathbf{\Phi}}_{i,m}(\mathbf{s}_{i,m} + \mathbf{n}_{i,m}) \text{ and } \|\hat{\mathbf{\Phi}}_{i,m}\|_2 = 1\end{aligned} \tag{29}$$

where $I(y_{i,m};\mathbf{s}_{i,m})$ denotes the mutual information between the measurement $y_{i,m}$ and the FHSS signal $\mathbf{s}_{i,m}$. In other words, the goal of the measurement kernel design is to maximize the information about the signal in the measurements. The mutual information metric in (29) can be expanded as:

$$I(y_{i,m};\mathbf{s}_{i,m}) = h(y_{i,m}) - h(y_{i,m}|\mathbf{s}_{i,m}). \tag{30}$$

We note that the conditional differential entropy term $h(y_{i,m}|\mathbf{s}_{i,m})$ depends only on the noise power when $\|\hat{\mathbf{\Phi}}_{i,m}\|_2 = 1$ and has no effect on the maximization problem of (29) for a given noise level. This can be seen by considering the conditional differential entropy:

$$\begin{aligned}h(y_{i,m}|\mathbf{s}_{i,m}) &= h((\hat{\mathbf{\Phi}}_{i,m}\mathbf{n}_{i,m} + \hat{\mathbf{\Phi}}_{i,m}\mathbf{s}_{i,m})|\hat{\mathbf{\Phi}}_{i,m}\mathbf{s}_{i,m}) \\ &= h(\hat{\mathbf{\Phi}}_{i,m}\mathbf{n}_{i,m}).\end{aligned} \tag{31}$$

When $\|\hat{\mathbf{\Phi}}_{i,m}\|_2 = 1$, $\hat{\mathbf{\Phi}}_{i,m}\mathbf{n}_{i,m}$ is a zero-mean circularly-symmetric jointly-Gaussian complex random vector and, thus, $h(y_{i,m}|\mathbf{s}_{i,m})$ depends only on the noise power. Therefore, an equivalent form of (29) can be given as:

$$\begin{aligned}\mathbf{\Phi}_{i,m} &= \arg\max_{\hat{\mathbf{\Phi}}_{i,m}} h(y_{i,m}) \\ \text{s.t. } y_{i,m} &= \hat{\mathbf{\Phi}}_{i,m}(\mathbf{s}_{i,m} + \mathbf{n}_{i,m}) \text{ and } \|\hat{\mathbf{\Phi}}_{i,m}\|_2 = 1.\end{aligned} \tag{32}$$

The problem represented by (32) can be computationally challenging to solve for arbitrary signals. To achieve a

computationally efficient solution, we utilize a mixture-of-Gaussian (MoG) model to represent the FHSS signal. MoG distributions are commonly used in signal processing applications since they allow accurate description of many real-world signals and are often mathematically tractable. Recently, there has also been interest in using MoG models in CS applications [47]–[51]. In our application, the use of the MoG model allows efficient solution of the problem in (32) through the use of a closed-form gradient approximation. In our model, we uniformly divide the FHSS hopping range into N_{b} subbands. Within each subband, the distribution of the FHSS signal is modeled as a complex zero-mean Gaussian white signal with variance σ_{s}^2. This MoG distribution is given by:

$$g(\mathbf{s}_{i,m}) = \sum_{l=1}^{N_{\mathrm{b}}} w_l \, \mathcal{CN}(\mathbf{0}, \mathbf{C}_{\mathrm{ss}}^{(l)}) \tag{33}$$

where w_l denotes the weight of the l^{th} Gaussian component, and $\mathcal{CN}(\mathbf{0}, \mathbf{C}_{\mathrm{ss}}^{(l)})$ denotes the probability density function of a complex zero-mean white Gaussian random variable within the l^{th} subband, and $\mathbf{C}_{\mathrm{ss}}^{(l)}$ denotes the corresponding covariance matrix. Since the l^{th} component of the MoG represents the FHSS signal within the l^{th} subband as a complex zero-mean Gaussian white signal with variance σ_{s}^2 within the subband, the covariance $\mathbf{C}_{\mathrm{ss}}^{(l)}$ can be calculated by computing the product of the autocorrelation of the impulse response of the ideal bandpass filter with its passband as the l^{th} subband and the variance σ_{s}^2. It can be seen that each component in this MoG model represents the FHSS signal in one of the N_{b} subbands.

Given this MoG model, additive white Gaussian noise, and the constraint that the rows of $\mathbf{\Phi}_i$ are normalized, it can be shown that the problem in (32) can be further reduced to:

$$\begin{aligned} \mathbf{\Phi}_{i,m} &= \arg\max_{\hat{\mathbf{\Phi}}_{i,m}} h(y_{i,m}|H_1) \\ &\text{s.t. } \|\hat{\mathbf{\Phi}}_{i,m}\|_2 = 1 \end{aligned} \tag{34}$$

where $h(y_{i,m}|H_1)$ denotes the entropy of the measurement in the signal present case. Details of the derivations used to obtain this result are given in the Appendix. In order to solve (34), an iterative gradient method is implemented. At each iteration, $\mathbf{\Phi}_{i,m}$ is refined using:

$$\begin{aligned} \mathbf{X} &= \mathbf{\Phi}_{i,m}^{(j)} + \mu \nabla_{\mathbf{\Phi}_{i,m}} h(y_{i,m}|H_1) \\ \mathbf{\Phi}_{i,m}^{(j+1)} &= \frac{\mathbf{X}}{\|\mathbf{X}\|_2} \end{aligned} \tag{35}$$

where $\mathbf{\Phi}_{i,m}^{(j)}$ and $\mathbf{\Phi}_{i,m}^{(j+1)}$ denote the non-zero entries of the m^{th} row of $\mathbf{\Phi}_i$ after j and $j+1$ iterations, respectively, and μ denotes the step size. An approximation to the gradient term $\nabla_{\mathbf{\Phi}_{i,m}} h(y_{i,m}|H_1)$ is provided in the Appendix.

A. Prior Knowledge Enhanced Measurement Kernel Design

In the above derivations, both the conditional entropy $h(y_{i,m}|H_1)$ and its gradient $\nabla_{\mathbf{\Phi}_{i,m}} h(y_{i,m}|H_1)$ are functions of the signal distribution which was modeled as an MoG distribution. In this MoG signal model, the weights of the Gaussian components w_l for $1 \le l \le N_{\mathrm{b}}$ are taken to be the subband occupancy probabilities of the FHSS signal. Given these weights of the Gaussian components w_l, optimized measurement kernels can be designed using (34) and (35). Here, we assume that the subband usage probabilities of the FHSS signal do not change over time. Thus, the measurement kernels are designed once and used repeatedly throughout the observation process. More specifically, (34) and (35) can be used to design the non-zero entries $\mathbf{\Phi}_{i,m}$ in the m^{th} row of the measurement matrix $\mathbf{\Phi}_i$ for $1 \le m \le M$. After all its rows are designed, the measurement matrix $\mathbf{\Phi}_i$ is used repeatedly during the entire observation process. In other words, in this case, the measurement matrix $\mathbf{\Phi}_i$ is constant across all observation intervals indexed by i.

B. Adaptive Measurement Kernel Design

The method described in the previous subsection can be used to exploit the non-uniformity of the subband usage probabilities to obtain optimized compressive measurement kernels. While this may be of interest in some limited applications, the subband usage probabilities in most FHSS applications are uniform. Therefore, there may not be significant non-uniformity in the probabilities to exploit. However, the framework described above lays the foundation for adaptive compressive measurements. In this approach, the measurement kernels $\mathbf{\Phi}_{i,m}$ are designed adaptively. After each measurement, a posterior probability distribution of subband usage under the signal present assumption is calculated using all previous measurements, which is often non-uniform. These posterior probabilities are used to replace the Gaussian component weights w_l in the above framework and a new measurement kernel that will be used during the next observation interval is obtained. To calculate the posterior probabilities, prior probabilities obtained from the previous measurement periods and likelihood values computed using the measurements from the current measurement period are used.

V. Results

Both theoretical analysis and simulations using practical FHSS signals were performed to evaluate and compare the detection performances of the systems discussed in the previous sections. These results are presented in this section.

A. Theoretical Detection Performance

We first compare the performances of the conventional detection system based on SSA and the compressive detection system with random measurement kernels. The theoretical FNR (i.e. probability of miss) calculated using the formulas derived earlier in this paper versus signal-to-noise ratio (SNR) is shown in Fig. 3. Here, the SNR is defined as:

$$\mathrm{SNR} = \frac{\sigma_{\mathrm{s}}^2}{\sigma_{\mathrm{n}}^2}. \tag{36}$$

In addition to the SSA and the proposed compressive detection with random measurement kernels, a clairvoyant system with knowledge of the FHSS hopping sequence was also implemented as reference. The clairvoyant system used measurement

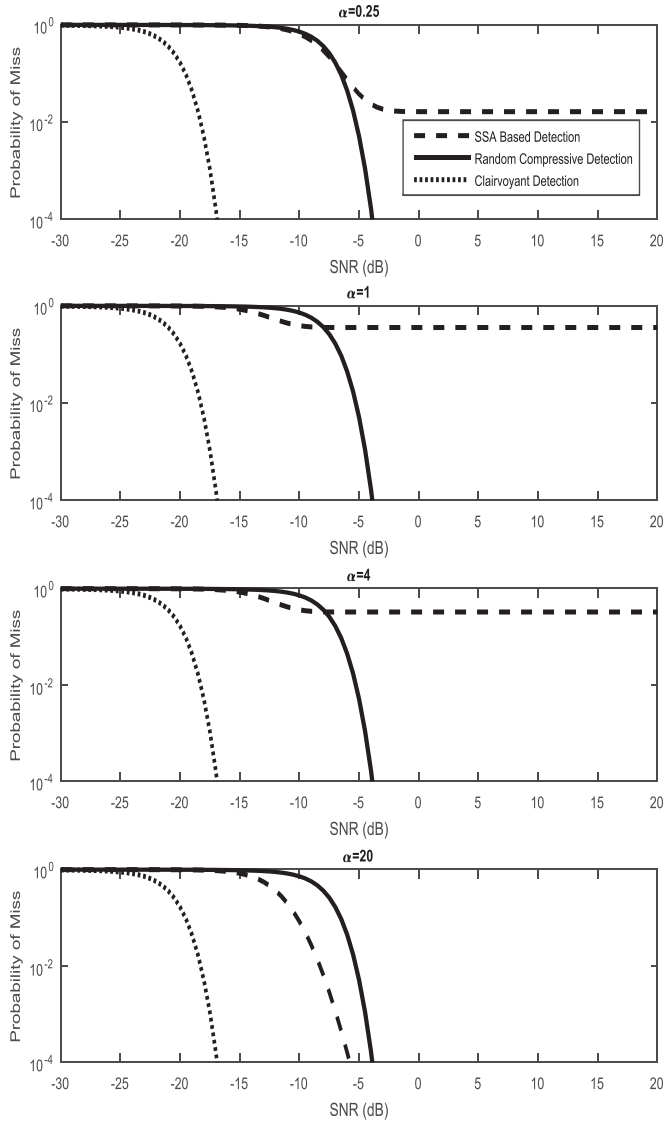

Fig. 3. Comparison of theoretical FHSS detection performances of different detection systems. α is the relative scanning/measurement rate, i.e., the number of scanning intervals (the SSA based detection system) or observation intervals (compressive detection systems) per FHSS hopping period.

kernels focused on the subband that the FHSS signal occupied at any given time. Although unpractical, the clairvoyant system serves as a benchmark in the presented results. In Fig. 3, the plots corresponding to four different α (relative scanning rate in the SSA based detection system and relative measurement rate in compressive detection systems) values are shown. The thresholds in the systems were obtained by setting the overall theoretical FPRs to 0.01: for SSA, the thresholds T_i's were calculated by solving (8) with equal FPR_i values for $1 \leq i \leq N_\text{b}$, so that $\text{FPR}_i = 1 - (1 - \text{FPR})^{\frac{1}{N_\text{b}}}$ according to (9); and for the compressive detection system, the threshold T was calculated by solving (27). The results in this figure are for uniform channel usage of the FHSS signal, and correspond to parameters $CR = N_\text{b} = 20$ and $M = 16$.

In Fig. 3, it is shown that the clairvoyant system, although unpractical, has the lowest probability of miss at all SNR and α values and serves as a benchmark. It is also shown that the conventional detection system based on SSA suffers from an evident "floor" in its FNR at high SNR values, if the relative scanning rate is not high enough. This floor results from the non-zero probability that the scanning support of SSA misses the hopping frequency of the FHSS signal in those cases. It can also be observed that the compressive detection system with random measurement kernels has slightly higher FNR than the SSA based system at low SNR values due to the Noise Folding effect [52]. However, the compressive detection system does not suffer from the FNR "floor" problem as in the SSA based system and has a better performance than the SSA based system over a large range of SNR values.

B. Detection Performance from Simulations

A Monte-Carlo simulation study was also conducted to compare the performances of the SSA and the proposed compressive detection with random measurement kernels. The FNR versus SNR obtained in these simulations are shown in Fig. 4. The FHSS signals used in these simulations were similar to those specified by the Bluetooth standard [53]. Bluetooth signals are obtained by combining Gaussian frequency-shift keying modulation of binary symbols with FHSS. The standard specifies 79 channels with 1 MHz channel bandwidth distributed between 2.402 GHz and 2.480 GHz. In order to match the simulation setup to the theoretical analysis setup, we set $N_\text{b} = 20$. We specified 80 frequency channels and left the last channel unused. As a result, the number of frequency channels covered by a scanning subband was set to 4. Four symbol periods were taken as a scanning interval in the SSA based detection system and an observation interval in the compressive detection system. Therefore, the number of Nyquist samples in each scanning/observation interval was 320. Different α values were obtained by varying the number of symbol periods per scanning/observation interval. The clairvoyant system with knowledge of the FHSS hopping sequence was also implemented as reference. A whitening step was applied to the measurements in the SSA and clairvoyant systems to counter the correlation introduced by the non-ideal filters used in the simulations. In the compressive detection system, CR was set to 20 so that the number of measurements during an observation interval in the compressive detection system is equal to the number of measurements during a scanning interval in the SSA based detection system. The same thresholds used in theoretical analysis were used in these simulations so that the overall theoretical FPRs were 0.01. 10^6 Monte-Carlo simulations were performed to generate each point in the curves of Fig. 4.

In Fig. 4, we can see that the simulated performances of the clairvoyant and the compressive detection systems match well with the results obtained by theoretical analysis in Fig. 3. However, the FNR "floor" problem in the SSA based system is somewhat reduced in Fig. 4. This happens because of the usage of non-ideal filters in the practical simulations. With non-ideal filters, the signals outside the passband of the filters were not completely stopped. This unintentional leakage improves the detection performance of the SSA based detection system.

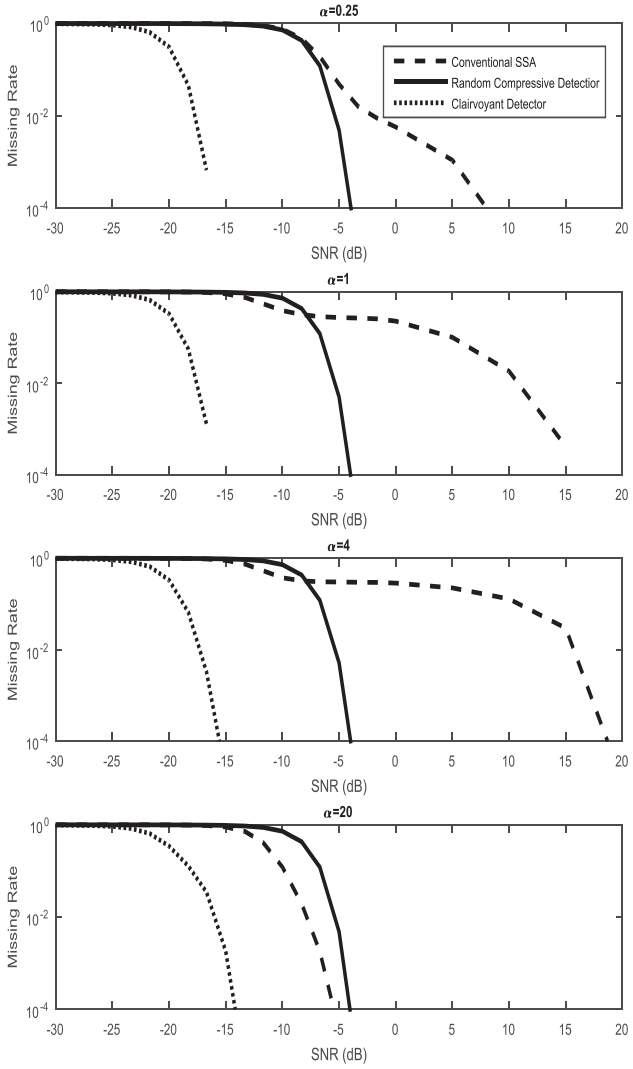

Fig. 4. Comparison of simulated FHSS Detection Performances of Different Detection Systems. α is the relative scanning/measurement rate, i.e., the number of scanning intervals (the SSA based detection system) or observation intervals (compressive detection systems) per FHSS hopping period.

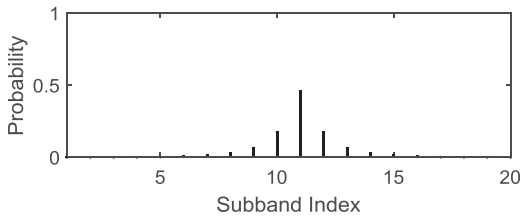

Fig. 5. Prior distribution of the subband occupation used in the experiments.

Next, we evaluate the performance of the compressive detection system with optimized measurement kernels using Monte Carlo simulations. Here, we considered the *static design* case where the measurement kernels were optimized once and used throughout the measurement process. The FHSS signals used in these simulations were almost the same as those used above except that we set $N_{\mathrm{b}} = 20$ when designing measurement kernels and the prior distribution of the subband occupation was no longer uniform but followed the distribution shown in Fig. 5. Similar to the experiments above, we set $CR = N_{\mathrm{b}}$ for the

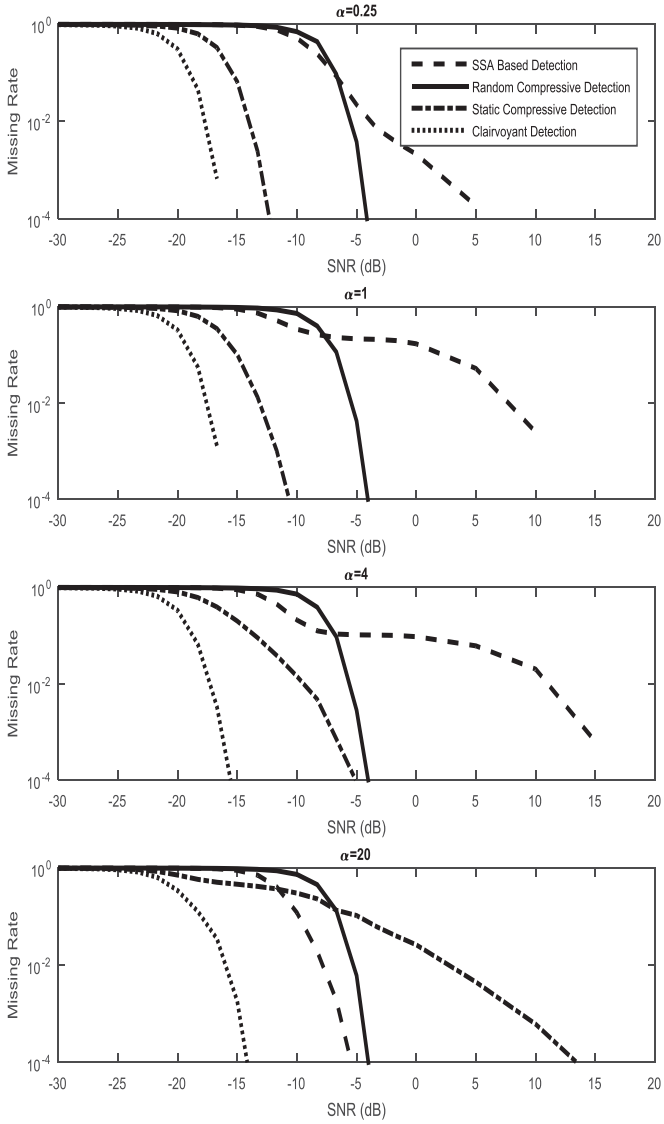

Fig. 6. Comparison of simulated FHSS detection performance of compressive detection system with prior knowledge enhanced measurement kernels with other detection systems. α is the relative scanning/measurement rate, i.e., the number of scanning intervals (the SSA based detection system) or observation intervals (compressive detection systems) per FHSS hopping period.

compressive detection methods and the same thresholds used in theoretical analysis were used in these simulations so that the overall theoretical FPRs were 0.01. The clairvoyant system with knowledge of the FHSS hopping sequence was also implemented as reference. The results are shown in Fig. 6, where 10^6 Monte-Carlo simulations were performed to generate each point in the curves.

In Fig. 6, the detection performance of the compressive detection system with prior knowledge enhanced measurement kernels is superior to that of the compressive detection system with random measurement kernels when the relative observation rate α is low. This improvement can be several orders of magnitude decrease in FNR. However, when the relative observation rate α is high, the performance of the compressive detection

system with prior knowledge enhanced measurement kernels gets worse. Especially when $\alpha \geq N_{\mathrm{b}}$ so that an FHSS hopping period covers the entire observation interval, the prior knowledge enhanced measurement kernels turn out to have worse performance than the random measurement kernels at high SNR values. This happens because as α increases, the spectra during the entire observation process becomes farther and farther away from that specified in Fig. 5. As a result, the support of the prior knowledge enhanced measurement kernels are more likely to miss the signal in these cases.

We also performed simulations using uniform prior subband usage distributions to design static measurement kernels. In this experiment, the measurement kernels were designed prior to the start of the measurement process and used throughout the measurement process. As expected, the detection performance obtained using these statically designed measurement kernels were the same as the performance of the random measurement kernels shown in Fig. 4.

The performance of the adaptive compressive detection approach was also evaluated using simulations. We compare the FNRs of the adaptive compressive detection approach to the compressive detection approach with random measurement kernels after each observation/scanning interval. The detection decisions were made at the end of each observation interval using all the measurements from the first observation interval to the current observation interval. In the adaptive measurement kernel design, we initialized the first row of the measurement kernel in the first observation interval $\mathbf{\Phi}_{1,1}$ to be from the prior knowledge enhanced measurement kernel assuming uniform subband occupation, and designed the remaining measurement kernels following (34) and (35). We used almost the same setup of the FHSS signals as those used to obtain the results in Fig. 4 except that we set the relative observation rate $\alpha = 20$ so that the frequency channel of the FHSS signal did not hop during the entire observation process. Therefore, the posterior distribution of the subband occupation of the FHSS signals remained valid since no frequency hopping took place. Similar to the simulations with prior knowledge enhanced measurement kernels, we set $CR = N_{\mathrm{b}} = 20$. However, the distribution of the subband occupation in these simulations was taken to be uniform. SNR was fixed to -5 dB. The simulation results are shown in Fig. 7. In the figure, *Dwell Time* denotes the number of observation intervals and 20 000 Monte-Carlo simulations were performed to generate each point in the curves. The thresholds were determined by setting the overall FPR to 0.01 using the measurements that had already been made: the threshold at the Dwell time DT was got by solving (28), with (25) replaced with:

$$p(\lambda|H_1) = \frac{\lambda^{(M\cdot DT-1)} e^{-\frac{\lambda}{{\sigma_{\mathrm{n}}}^2}}}{{\sigma_{\mathrm{n}}}^{2M\cdot DT}\Gamma(M\cdot DT)}. \tag{37}$$

In Fig. 7, we can observe that the FNR of the adaptive compressive detection system decreases faster than the compressive detection system with random measurement kernels. Therefore, much fewer observation intervals are needed for the adaptive compressive detection system to achive a particular FNR compared to the compressive detection system with random kernels.

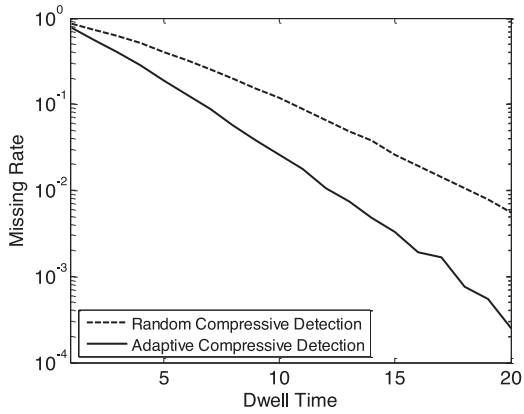

Fig. 7. Comparison of simulated FHSS detection performance of the adaptive compressive detection system with the random compressive detection system.

Similarly, after a given number of observation intervals, the adaptive compressive detection system has much lower FNR than the compressive detection system with random measurement kernels, and the improvement can be several orders in magnitude.

VI. Summary and Conclusion

In this paper, we proposed methods for non-cooperative compressive detection of FHSS signals. We introduced the FHSS detection problem and provided a model to analyze the theoretical performance of conventional SSA-based detection systems. We then introduced a compressive detection approach that uses random measurement kernels. In addition to the compressive detection system with random measurement kernels, we also introduced compressive detection systems with designed measurement kernels and illustrated how the measurement kernels can be adapted during the measurement process. The proposed detection methods were evaluated using both theoretical analysis and simulations using practical FHSS signals. The experimental results illustrated that the compressive detection systems do not suffer from the FNR "floor" problem which is observed in SSA based systems when the relative scanning rate is low and the SNR is high. In addition, experimental results also illustrate that prior (or posterior) knowledge of signal distribution can be used to design measurement kernels which yield enhanced detection performance compared to random measurement kernels.

Appendix
Derivations of the Compressive Measurement Kernel Design Method

In this Appendix, we provide the details of the derivations used to obtain (34) and (35). Recall that we modeled the FHSS signal by dividing the FHSS hopping range into N_{b} subbands and modeling the distribution of the FHSS signal by a complex zero-mean Gaussian white signal within each subband. This MoG distribution was given in (33). Given this MoG signal model and zero-mean additive Gaussian white noise with variance σ_{n}^2, the distribution of the m^{th} measurement during the i^{th}

observation interval $y_{i,m}$ is also an MoG distribution:

$$f(y_{i,m}) = P_{\rm s}\sum_{l=1}^{N_{\rm b}} w_l f_l(y_{i,m}) + (1-P_{\rm s}) f_0(y_{i,m}) \tag{38}$$

where $P_{\rm s}$ denotes the probability of signal present

$$f_0(y_{i,m}) = \mathcal{CN}(0, \sigma_{\rm n}^2 \mathbf{\Phi}_{i,m} \mathbf{I}_{CR} \mathbf{\Phi}_{i,m}^{\dagger}) \tag{39}$$

denotes the distribution of $y_{i,m}$ in the signal absent case, and

$$f_l(y_{i,m}) = \mathcal{CN}(0, \mathbf{\Phi}_{i,m} \mathbf{C}_{\rm xx}^{(l)} \mathbf{\Phi}_{i,m}^{\dagger}) \tag{40}$$

denotes the distribution of $y_{i,m}$ when the $l^{\rm th}$ subband is used in the signal present case with $\mathbf{C}_{\rm xx}^{(l)} = \mathbf{C}_{\rm ss}^{(l)} + \sigma_{\rm n}^2 \mathbf{I}_{CR}$ and $\mathbf{I}_{CR}$ denoting the $CR \times CR$ identity matrix.

Given this distribution, we can compute the differential entropy:

$$\begin{aligned} &h(y_{i,m}) \\ &= -\int f(y_{i,m}) \log[f(y_{i,m})] dy_{i,m} \\ &= -\int \left(P_{\rm s}\sum_{l=1}^{N_{\rm b}} w_l f_l(y_{i,m}) + (1-P_{\rm s}) f_0(y_{i,m}) \right) \\ &\quad \cdot \log \left[P_{\rm s}\sum_{l=1}^{N_{\rm b}} w_l f_l(y_{i,m}) + (1-P_{\rm s}) f_0(y_{i,m}) \right] dy_{i,m}. \end{aligned} \tag{41}$$

Approximating the term $\log[P_{\rm s}\sum_{l=1}^{N_{\rm b}} w_l f_l(y_{i,m}) + (1-P_{\rm s}) f_0(y_{i,m})]$ by the first two terms of its Taylor expansion at $E[y_{i,m}] = 0$, we get:

$$\begin{aligned} &\log \left[P_{\rm s}\sum_{l=1}^{N_{\rm b}} w_l f_l(y_{i,m}) + (1-P_{\rm s}) f_0(y_{i,m}) \right] \\ &= \log \left[P_{\rm s}\sum_{l=1}^{N_{\rm b}} w_l f_l(0) + (1-P_{\rm s}) f_0(0) \right] \\ &\quad + \nabla_{y_{i,m}} \left\{ \log \left[P_{\rm s}\sum_{l=1}^{N_{\rm b}} w_l f_l(y_{i,m}) \right. \right. \\ &\quad \left. \left. + (1-P_{\rm s}) f_0(y_{i,m}) \right] \right\} |_{y_{i,m}=0} \cdot y_{i,m} + \text{H.O.T.} \\ &\approx \log \left[P_{\rm s}\sum_{l=1}^{N_{\rm b}} w_l f_l(0) + (1-P_{\rm s}) f_0(0) \right] + G(0) \cdot y_{i,m} \end{aligned} \tag{42}$$

where H.O.T. denotes the higher order terms in the Taylor expansion and $G(0) = \nabla_{y_{i,m}} \{\log[P_{\rm s}\sum_{l=1}^{N_{\rm b}} w_l f_l(y_{i,m}) + (1-P_{\rm s}) f_0(y_{i,m})]\}|_{y_{i,m}=0}$.

Substituting (42) into (41), we get:

$$\begin{aligned} &h(y_{i,m}) \\ &\approx -\int \left(P_{\rm s}\sum_{l=1}^{N_{\rm b}} w_l f_l(y_{i,m}) + (1-P_{\rm s}) f_0(y_{i,m}) \right) \\ &\quad \left[\log \left[P_{\rm s}\sum_{l=1}^{N_{\rm b}} w_l f_l(0) + (1-P_{\rm s}) f_0(0) \right] + G(0) \cdot y_{i,m} \right] dy_{i,m} \\ &= -\log \left[P_{\rm s}\sum_{l=1}^{N_{\rm b}} w_l f_l(0) + (1-P_{\rm s}) f_0(0) \right] \\ &= -\log \left[P_{\rm s}\sum_{l=1}^{N_{\rm b}} \frac{w_l}{\pi(\mathbf{\Phi}_{i,m} \mathbf{C}_{\rm xx}^{(l)} \mathbf{\Phi}_{i,m}^{\dagger})} + \frac{1-P_{\rm s}}{\pi(\sigma_{\rm n}^2 \mathbf{\Phi}_{i,m} \mathbf{I}_{CR} \mathbf{\Phi}_{i,m}^{\dagger})} \right]. \end{aligned} \tag{43}$$

Similarly, the differential entropy of $y_{i,m}$ in the signal present case is calculated by:

$$h(y_{i,m}|H_1) \approx -\log \left[\sum_{l=1}^{N_{\rm b}} \frac{w_l}{\pi(\mathbf{\Phi}_{i,m} \mathbf{C}_{\rm xx}^{(l)} \mathbf{\Phi}_{i,m}^{\dagger})} \right]. \tag{44}$$

When the probability of signal present $P_{\rm s}$ is fixed and given the constraint that $\mathbf{\Phi}_{i,m}$ are normalized, the second term inside the summation in (43) is a constant. Therefore, maximizing the entropy $h(y_{i,m})$ is equivalent to maximizing the conditional entropy $h(y_{i,m}|H_1)$.

To obtain the gradient $\nabla_{\mathbf{\Phi}_{i,m}} h(y_{i,m}|H_1)$, we use the chain rule for the derivatives:

$$\begin{aligned} &\nabla_{\mathbf{\Phi}_{i,m}} h(y_{i,m}|H_1) \\ &\approx \nabla_{\mathbf{\Phi}_{i,m}} \left\{ -\log \left[\sum_{l=1}^{N_{\rm b}} \frac{w_l}{\pi(\mathbf{\Phi}_{i,m} \mathbf{C}_{\rm xx}^{(l)} \mathbf{\Phi}_{i,m}^{\dagger})} \right] \right\} \\ &= -\frac{\sum_{l=1}^{N_{\rm b}} w_l \pi^{-1} \nabla_{\mathbf{\Phi}_{i,m}} \{(\mathbf{\Phi}_{i,m} \mathbf{C}_{\rm xx}^{(l)} \mathbf{\Phi}_{i,m}^{\dagger})^{-1}\}}{\sum_{l=1}^{N_{\rm b}} w_l \pi^{-1} (\mathbf{\Phi}_{i,m} \mathbf{C}_{\rm xx}^{(l)} \mathbf{\Phi}_{i,m}^{\dagger})^{-1}} \\ &= \frac{\sum_{l=1}^{N_{\rm b}} w_l \pi^{-1} (\mathbf{\Phi}_{i,m} \mathbf{C}_{\rm xx}^{(l)} \mathbf{\Phi}_{i,m}^{\dagger})^{-2} \mathbf{\Phi}_{i,m} \mathbf{C}_{\rm xx}^{(l)\dagger}}{\sum_{l=1}^{N_{\rm b}} w_l \pi^{-1} (\mathbf{\Phi}_{i,m} \mathbf{C}_{\rm xx}^{(l)} \mathbf{\Phi}_{i,m}^{\dagger})^{-1}} \\ &= \frac{\sum_{l=1}^{N_{\rm b}} w_l (\mathbf{\Phi}_{i,m} \mathbf{C}_{\rm xx}^{(l)} \mathbf{\Phi}_{i,m}^{\dagger})^{-2} \mathbf{\Phi}_{i,m} \mathbf{C}_{\rm xx}^{(l)\dagger}}{\sum_{l=1}^{N_{\rm b}} w_l (\mathbf{\Phi}_{i,m} \mathbf{C}_{\rm xx}^{(l)} \mathbf{\Phi}_{i,m}^{\dagger})^{-1}}. \end{aligned} \tag{45}$$

REFERENCES

[1] J. Proakis, *Digital Communications*, 4th ed. New York, NY, USA: McGraw-Hill, 2000.

[2] M. Fargues, H. Overdyk, and R. Hippenstiel, "Wavelet-based detection of frequency hopping signals," in *Proc. Conf. Rec. 31st Asilomar Conf. Signals, Syst. Amp; Comput.*, 1997, vol. 1, pp. 515–519.

[3] J. Hampton and J. Oetting, "A frequency hopping sequential detection technique for in-net coarse acquisition," in *Proc. IEEE Mil. Commun. Conf.*, 1992, vol. 1, pp. 43–47.

[4] H. Fan, Y. Guo, and Y. Xu, "A novel algorithm of blind detection of frequency hopping signal based on second-order cyclostationarity," in *Proc. Congr. Image Signal Process.*, 2008, vol. 5, pp. 399–402.

[5] A. Polydoros and K. Woo, "LPI detection of frequency-hopping signals using autocorrelation techniques," *IEEE J. Sel. Areas Commun.*, vol. 3, no. 5, pp. 714–726, Sep. 1985.

[6] J. Lv and W. Qu, "Application of the wavelet rearrangement algorithm in the detection of noncooperative frequency hopping signals," in *Proc. IEEE 11th Int. Conf. Signal Process.*, 2012, vol. 1, pp. 263–266.

[7] M. Sirotiya and A. Banerjee, "Detection and estimation of frequency hopping signals using wavelet transform," in *Proc. 2nd UK-India-IDRC Int. Workshop Cogn. Wireless Syst.*, 2010, pp. 1–5.

[8] H. F. Overdyk, "Detection and estimation of frequency hopping signals using wavelet transforms," Ph.D. dissertation, Naval Postgraduate School, Monterey, CA, USA, 1997.

[9] K. Jaiswal, "Spectral sensing for cognitive radio: Estimation of adaptive frequency hopping signal," in *Proc. IEEE Region 10 Conf.*, 2008, pp. 1–5.

[10] K. Jaiswal, "Spectral sensing of adaptive frequency hopping signal for cognitive radio," in *Proc. IEEE Int. Performance, Comput. Commun. Conf.*, 2008, pp. 360–365.

[11] C. D. Chung, "Generalised likelihood-ratio detection of multiple-hop frequency-hopping signals," *IEEE Proc. Commun.*, vol. 141, no. 2, pp. 70–78, Apr. 1994.

[12] C. D. Chung, "Generalized likelihood-ratio detection of multiple-hop frequency-hopping signals," in *Proc. IEEE Mil. Commun. Conf.*, 1991, vol. 2, pp. 527–531.

[13] R. Dillard and G. Dillard, "Likelihood-ratio detection of frequency-hopped signals," *IEEE Trans. Aerosp. Electron. Syst.*, vol. 32, no. 2, pp. 543–553, Apr. 1996.

[14] B. Levitt, U. Cheng, A. Polydoros, and M. Simon, "Optimum detection of slow frequency-hopped signals," *IEEE Trans. Commun.*, vol. 42, no. 234, pp. 1990–2000, Feb.–Apr. 1994.

[15] B. Levitt, M. Simon, A. Polydoros, and U. Cheng, "Partial-band detection of frequency-hopped signals," in *Proc. IEEE Global Telecommun. Conf.*, 1993, vol. 4, pp. 70–76.

[16] W. Snelling and E. Geraniotis, "Sequential detection of unknown frequency-hopped waveforms," *IEEE J. Sel. Areas Commun.*, vol. 7, no. 4, pp. 602–617, May 1989.

[17] H. Luan and H. Jiang, "Blind detection of frequency hopping signal using time-frequency analysis," in *Proc. 6th Int. Conf. Wireless Commun. Netw. Mobile Comput.*, 2010, pp. 1–4.

[18] S. Luo and L. Luo, "Adaptive detection of an unknown FH signal based on image features," in *Proc. 5th Int. Conf. Wireless Commun. Netw. Mobile Comput.*, 2009, pp. 1–4.

[19] S. Luo and L. Luo, "Detection of an unknown frequency hopping signal based on image features," in *Proc. 2nd Int. Congr. Image Signal Process.*, 2009, pp. 1–4.

[20] J. Weber, K. Kowalske, C. Robertson, F. Kragh, and C. Brown, "Detection of frequency-hopped waveforms embedded in interference waveforms with noise," in *Proc. IEEE Int. Conf. Commun.*, 2007, pp. 2973–2978.

[21] F. Javed and A. Mahmood, "The use of time frequency analysis for spectrum sensing in cognitive radios," in *Proc. 4th Int. Conf. Signal Process. Commun. Syst.*, 2010, pp. 1–7.

[22] L. Miller and J. Lee, "Frequency-hopping signal detection using partial band coverage," *IEEE Trans. Aerosp. Electron. Syst.*, vol. 29, no. 2, pp. 540–553, Apr. 1993.

[23] R. Dillard and G. G. M. Dillard, *Detectability of Spread-Spectrum Signals*. Norwood, MA, USA: Artech House, 1989.

[24] R. Dillard, "Detectability of spread-spectrum signals," *IEEE Trans. Aerosp. Electron. Syst.*, vol. AES-15, no. 4, pp. 526–537, Jul. 1979.

[25] J. J. Lehtomäki and M. Juntti, "Detection of frequency hopping signals using a sweeping channelized radiometer," *Signal Process.*, vol. 85, no. 10, pp. 2030–2043, 2005.

[26] J. Lehtomaki, M. Juntti, and H. Saarnisaari, "Detection of frequency hopping signals with a sweeping channelized radiometer," in *Proc. Conf. Rec. 38th Asilomar Conf. Signals, Syst. Comput.*, 2004, vol. 2, pp. 2178–2182.

[27] J. Joo, J. Won, C. Lee, S. Park, and K. Lee, "Detection of an unknown FH signal using scanning receiver and DF receiver in practical environments," in *Proc. IEEE Wireless Commun. Netw. Conf.*, 2007, pp. 1226–1230.

[28] M. Song and S. Wigginton, "Frequency hopping pattern detection in wireless ad hoc networks," in *Proc. Int. Conf. Inf. Technol., Coding Comput.*, 2005, vol. 2, pp. 633–638.

[29] J. Lehtomaki, *Analysis of Energy Based Signal Detection*. Oulu, Finland: Oulu Univ. Press, 2005.

[30] E. J. Candes, J. Romberg, and T. Tao, "Robust uncertainty principles: Exact signal reconstruction from highly incomplete frequency information," *IEEE Trans. Inf. Theory*, vol. 52, no. 2, pp. 489–509, Feb. 2006.

[31] D. Donoho, "Compressed sensing," *IEEE Trans. Inf. Theory*, vol. 52, no. 4, pp. 1289–1306, Apr. 2006.

[32] M. Davenport, M. Wakin, and R. Baraniuk, "Detection and estimation with compressive measurements," Dept. Elect. Comput. Eng., Rice Univ., Houston, TX, USA, Tech. Rep. TREE 0610, 2006.

[33] M. Duarte, M. Davenport, M. Wakin, and R. Baraniuk, "Sparse signal detection from incoherent projections," presented at the IEEE Int. Conf. Acoustics, Speech Signal Processing, Toulouse, France, May 2006.

[34] Z. Wang, G. Arce, and B. Sadler, "Subspace compressive detection for sparse signals," in *Proc. IEEE Int. Conf. Acoust., Speech Signal Process.*, Mar. 2008, pp. 3873–3876.

[35] J. Paredes, Z. Wang, G. Arce, and B. Sadler, "Compressive matched subspace detection," in *Proc. 17th Eur. Signal Process. Conf.*, Aug. 2009, pp. 120–124.

[36] V. Havary-Nassab, S. Hassan, and S. Valaee, "Compressive detection for wide-band spectrum sensing," in *Proc. IEEE Int. Conf. Acoust. Speech Signal Process.*, Mar. 2010, pp. 3094–3097.

[37] M. Davenport, P. Boufounos, M. Wakin, and R. Baraniuk, "Signal processing with compressive measurements," *IEEE J. Sel. Topics Signal Process.*, vol. 4, no. 2, pp. 445–460, Apr. 2010.

[38] J. Zou, Y. Li, and W. Dai, "Compressive detection with sparse random projections," *IEICE Commun. Exp.*, vol. 2, no. 7, pp. 287–293, Jul. 2013.

[39] J. Tropp, J. Laska, M. Duarte, J. Romberg, and R. Baraniuk, "Beyond Nyquist: Efficient sampling of sparse bandlimited signals," *IEEE Trans. Inf. Theory*, vol. 56, no. 1, pp. 520–544, Jan. 2010.

[40] H. Zhu and G. Giannakis, "Exploiting sparse user activity in multiuser detection," *IEEE Trans. Commun.*, vol. 59, no. 2, pp. 454–465, Feb. 2011.

[41] Y. Xie, Y. Eldar, and A. Goldsmith, "Reduced-dimension multiuser detection," *IEEE Trans. Inf. Theory*, vol. 59, no. 6, pp. 3858–3874, Jun. 2013.

[42] X. Li, A. Rueetschi, A. Scaglione, and Y. Eldar, "Compressive link acquisition in multiuser communications," *IEEE Trans. Signal Process.*, vol. 61, no. 12, pp. 3229–3245, Jun. 2013.

[43] J. Hong, W. Choi, and B. Rao, "Sparsity controlled random multiple access with compressed sensing," *IEEE Trans. Wireless Commun.*, vol. 14, no. 2, pp. 998–1010, Feb. 2015.

[44] F. Liu, M. Marcellin, N. Goodman, and A. Bilgin, "Compressive detection of multiple frequency-hopping spread spectrum signals," in *Proc. Data Compression Conf.*, Mar. 2014, pp. 415–415.

[45] A. Papoulis and S. Pillai, *Probability, Random Variables, and Stochastic Processes*, 4th ed. New York, NY, USA: McGraw-Hill, 2002.

[46] M. A. Neifeld, A. Ashok, and P. K. Baheti, "Task-specific information for imaging system analysis," *J. Opt. Soc. Amer. A*, vol. 24, no. 12, pp. B25–B41, 2007.

[47] Y. Gu, N. Goodman, and A. Ashok, "Radar target profiling and recognition based on TSI-optimized compressive sensing kernel," *IEEE Trans. Signal Process.*, vol. 62, no. 12, pp. 3194–3207, Jun. 2014.

[48] G. Yu and G. Sapiro, "Statistical compressive sensing of Gaussian mixture models," in *Proc. IEEE Int. Conf. Acoust., Speech Signal Process.*, May 2011, pp. 3728–3731.

[49] G. Yu, G. Sapiro, and S. Mallat, "Solving inverse problems with piecewise linear estimators: From Gaussian mixture models to structured sparsity," *IEEE Trans. Image Process.*, vol. 21, no. 5, pp. 2481–2499, May 2012.

[50] J. Wu, F. Liu, L. Jiao, X. Wang, and B. Hou, "Multivariate compressive sensing for image reconstruction in the wavelet domain: Using scale mixture models," *IEEE Trans. Image Process.*, vol. 20, no. 12, pp. 3483–3494, Dec. 2011.

[51] J. Duarte-Carvajalino, G. Yu, L. Carin, and G. Sapiro, "Task-driven adaptive statistical compressive sensing of Gaussian mixture models," *IEEE Trans. Signal Process.*, vol. 61, no. 3, pp. 585–600, Feb. 2013.

[52] E. Arias-Castro and Y. C. Eldar, "Noise folding in compressed sensing," *IEEE Signal Process. Lett.*, vol. 18, no. 8, pp. 478–481, Aug. 2011.

[53] IEEE 802.15, *Specification of the Bluetooth System*, Dec. 1, 1999. [Online]. Available: http://grouper.ieee.org/groups/802/15/Bluetooth/profile_10_b.pdf, last accessed August 8, 2016.

[54] F. Liu, M. Marcellin, N. Goodman, and A. Bilgin, "Compressive detection of frequency-hopping spread spectrum signals," in *Proc. SPIE, Compressive Sens. II*, 2013, vol. 8717, pp. 87 170P–87 170P–6. [Online]. Available: http://dx.doi.org/10.1117/12.2015969

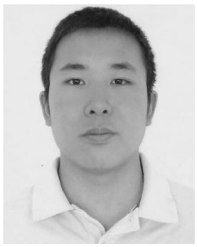

Feng Liu received the B.S. degree in electronic information science and technology from Nankai University, Tianjin, China, in 2008, and the Ph.D. degree in electrical and computer engineering from the University of Arizona, Tucson, AZ, USA, in 2015. He is currently a Postdoctoral Research Associate in the Department of Electrical and Computer Engineering, University of Arizona. His research interests include signal and image processing, communications, data compression, and medical imaging.

Michael W. Marcellin (S'81–M'87–SM'93–F'02) received the B.S. degree from San Diego State University, San Diego, CA, USA, in 1983, and the M.S. and Ph.D. degrees from Texas A&M University, College Station, TX, USA, in 1985 and 1987, respectively.

Since 1988, he has been with the University of Arizona, where he holds the title of Regents Professor of Electrical and Computer Engineering. He was a major contributor to JPEG2000. He is a coauthor of the book: *JPEG2000: Image Compression Fundamentals, Standards and Practice* (Kluwer, 2001) and wrote the compression specification that is currently used for the distribution and exhibition of digital cinema. He is a College of Engineering Faculty Fellow (Teaching), and a University of Arizona Honors Professor.

Prof. Marcellin is a Member of Tau Beta Pi and Eta Kappa Nu. He received the National Science Foundation Young Investigator Award, the IEEE Signal Processing Society Senior (Best Paper) Award, and teaching awards from NTU in 1990 and 2001, IEEE/Eta Kappa Nu Student Section in 1997, and the University of Arizona College of Engineering in 2000, 2010, 2013, 2015, and 2016. In 2003, he was named the San Diego State University Distinguished Engineering Alumnus.

Nathan A. Goodman (S'98–M'02–SM'07) received the B.S., M.S., and Ph.D. degrees in electrical engineering from the University of Kansas, Lawrence, KS, USA, in 1995, 1997, and 2002, respectively. From 1996 to 1998, he was an RF Systems Engineer for Texas Instruments, Dallas, TX, USA. From 1998 to 2002, he was a Graduate Research Assistant in the Radar Systems and Remote Sensing Laboratory, University of Kansas. From 2002 to 2011, he was a Faculty Member in the ECE Department, University of Arizona, Tucson, AZ, USA, and is now a Professor in the School of Electrical and Computer Engineering and the Director of Research for the Advanced Radar Research Center, University of Oklahoma, Norman, OK, USA.

He has served as a Technical Cochair for the 2011 IEEE Radar Conference, a Finance Chair for the 2012 SAM Workshop, and an Associate Editor-in-Chief for the Elseviers *Digital Signal Processing* journal. He is currently an Associate Editor for IEEE TRANSACTIONS ON AEROSPACE AND ELECTRONIC SYSTEMS and a General Cochair for the 2018 IEEE Radar Conference. He also serves as a Cochair for the NATO SET-227 research task group on cognitive radar, a Lecturer for the SET-216 lecture series on Cognition and Radar Sensing, and as a Member of the IEEE AES Radar Systems Panel. His research interests include radar and array signal processing. He received the Madison A. and Lila Self Graduate Fellowship from the University of Kansas in 1998. He also received the IEEE 2001 International Geoscience and Remote Sensing Symposium Interactive Session Prize Paper Award.

Ali Bilgin (S'94–M'03–SM'08) received the B.S. degree in electronics and telecommunications engineering from Istanbul Technical University, Istanbul, Turkey, in 1992, the M.S. degree in electrical engineering from San Diego State University, San Diego, CA, USA, in 1995, and the Ph.D. degree in electrical engineering from the University of Arizona, Tucson, AZ, USA, in 2002. He is currently an Associate Professor in the Department of Biomedical Engineering, Department of Electrical and Computer Engineering, and Department of Medical Imaging, University of Arizona. He has authored or coauthored more than 175 research papers in international journals and conferences. He holds ten granted and several pending patents. He was on the Organizing Committees of many conferences, an Associate Editor of the IEEE SIGNAL PROCESSING LETTERS from 2010 to 2012, and the IEEE TRANSACTIONS ON IMAGE PROCESSING from 2010 to 2014. He is currently an Associate Editor of the IEEE TRANSACTIONS ON COMPUTATIONAL IMAGING. His research interests include signal and image processing, image and video coding, data compression, and magnetic resonance imaging.